Electron Microscopy Study of a New Cation Deficient Perovskite-like Oxide: $Ba_3MoNbO_{8.5}$

E. García-González, M. Parras, and J. M. González-Calbet*

Departamento Química Inorgánica, Facultad de Ciencias Químicas, Universidad Complutense de Madrid, 28040 Madrid, Spain

Received December 16, 1997. Revised Manuscript Received March 11, 1998

A new ordering scheme in cationic-deficient perovskite-like phases of the $Ba_n(Mo,Nb)_{n-\delta}O_{3n-x}$ system has been described for the composition $Ba_3MoNbO_{8.5}$, which has an oxygen stoichiometry between those of the 9R polytype and the palmierite structure. An electron diffraction and high-resolution electron microscopy study shows that the oxygen defect with respect to the 9R polytype $(hhc)_3$ leads to an ordered distribution of octahedra and tetrahedra in a 3:2 ratio in the cubic layers. The flexibility of the $(hhc)_3$ stacking sequence allows the formation of a modulated structure through an ordered shearing mechanism along **c** by introducing mixed $BaO_{2.6}$ cubic layers in the 9R polytype.

Introduction

The relative simplicity of the perovskite structure can be described in a useful way from the cubic stacking of compact hexagonal $[AO_3]$ layers, where the B cations occupy the octahedral cavities in a certain ratio leading to ABO_3. The alternation of cubic (c) and hexagonal (h) stacking of the layers in different percentages gives rise to the various hexagonal polytypes, and if the stacking sequence contains hexagonal triplets, chains of face-sharing octahedra must exist in the structure. The stability of such structures may occur by the formation of metal−metal bonds, by the location of B cations with small formal charges, or by the partial occupation of the octahedral cavities by atoms with large formal charge and cation vacancies.

In this sense, the structure adopted by hexagonal perovskite-like oxides with the general formula $A_nB_{n-\delta}O_{3n-x}$ ($\delta \geq 1$, $x \geq 0$) is related to the number of cationic vacancies in such a way that they are placed between two adjacent AO_3 hexagonally stacked layers.

Different systems have been explored, diverse terms being isolated: $La_nTi_{n-\delta}O_{3n}$,[1,2] $(A,La)_nTi_{n-\delta}RuO_{3n}$,[2,3] $Ba_n(Nb,Ti)_{n-\delta}O_{3n}$ and $Ba_n(Ta,Ti)_{n-\delta}O_{3n}$,[4−6] and $(Ba,La)_nNb_{n-\delta}O_{3n}$ and $La_n(Nb,W)_{n-\delta}O_{3n}$.[7,8] The building principles relating in a direct way composition and stacking sequences have been discussed extensively for the La−Ti−O system.[9]

It is a general fact that the composition of the B sublayer determines δ, which is itself determined by the type of close packing of AO_3 layers.[5,9] At the same time, the relative stability of the different polyhedral arrangements of the B framework makes possible or not the localization of oxygen vacancies.

Following these ideas, we have investigated the system $Ba_n(Mo,Nb)_{n-\delta}O_{3n-x}$, and our study shows the existence of $Ba_3MoNbO_{8.5}$ as a new cation-deficient perovskite-like ordered phase.

In the case of an A:B 3:2 cationic ratio, i.e., an $A_3B_2O_9$ composition, one of every three B sites remains unoccupied and two polytypes can be found: the $Cs_3Tl_2O_9$-type[10] where the empty octahedron is situated between face-sharing octahedra, and the 9R-type structure,[11,12] where the vacant octahedron is located between corner-sharing octahedra. For the anion-deficient composition $A_3B_2O_8$, the structure adopted is palmierite-type,[13] which can be described as a mixed-layer compound derived from the 9R type in the sense that the cubic layer c of this polytype with composition BaO_3 has been replaced by a BaO_2 layer in the $(hhc)_3$ sequence; this results in the creation of two tetrahedra separated by one unoccupied octahedron.

It is known that $Ba_3Nb_2O_8$ crystallizes with the palmierite structure, and during the course of this work, we have stated that $Ba_3Mo_2O_9$ is isostructural with $Ba_3W_2O_9$. The introduction of molybdenum and niobium in a 1:1 ratio originates the $O_{8.5}$ nominal composition, and the possibility of accommodation of this oxygen nonstoichiometry is the subject of the present study.

* To whom correspondence should be adressed.

(1) Fedorov, N. F.; Melnikova, O. V.; Saltykova, V. A.; Chistyakova, M. V. *Russ. J. Inorg. Chem.* **1979**, *24*, 1166.
(2) German, M.; Kovba, L. M. *Russ. J. Inorg. Chem.* **1980**, *28*, 2377.
(3) Bontchev, R.; Weill, F.; Darriet, J. *Mater. Res. Bull.* **1992**, *27*, 931.
(4) Mössner, B.; Kemmler-Sack, S.; *J. Less-Common Met.* **1986**, *120*, 203.
(5) Shpanchenko, R. V.; Nistor, L.; Van Tendeloo, G.; Van Landuyt, J.; Amelinckx, S.; Abakumov, A. M.; Antipov, E. V.; Kovba, L. M. *J. Solid State Chem.* **1995**, *114*, 560.
(6) Abakumov, A. M.; Van Tendeloo, G.; Scheglov, A. A.; Shpanchenko, R. V.; Antipov, E. V. *J. Solid State Chem.* **1996**, *125*, 102.
(7) Rother, H. J.; Kemmler-Sack, S.; Treiber, U.; Cyris, W. R. *Z. Anorg. Allg. Chem.* **1980**, *466*, 131.
(8) Kemmler-Sack, S.; Treiber, U. *Z. Anorg. Allg. Chem.* **1981**, *478*, 198.
(9) Van Tendeloo, G.; Amelinckx, S.; Darriet, B.; Bontchev, R.; Darriet, J.; Weill, F. *J. Solid State Chem.* **1994**, *108*, 314.
(10) Poeppelmeier, K. R.; Jacobson, A. J.; Longo, J. M. *Mater. Res. Bull.* **1980**, *15*, 339.
(11) Donohue, P.; Katz, L.; Ward, R. *Inorg. Chem.* **1965**, *4*, 306.
(12) Calvo, C.; Ng, H. N.; Chamberland, B. L. *Inorg. Chem.* **1978**, *17*, 699.
(13) Longo, J. M.; Clavenna, L. R. *Ann. N.Y. Acad. Sci.* **1976**, *272*, 45.

S0897-4756(97)00802-8 CCC: $15.00
Published on Web 05/21/1998

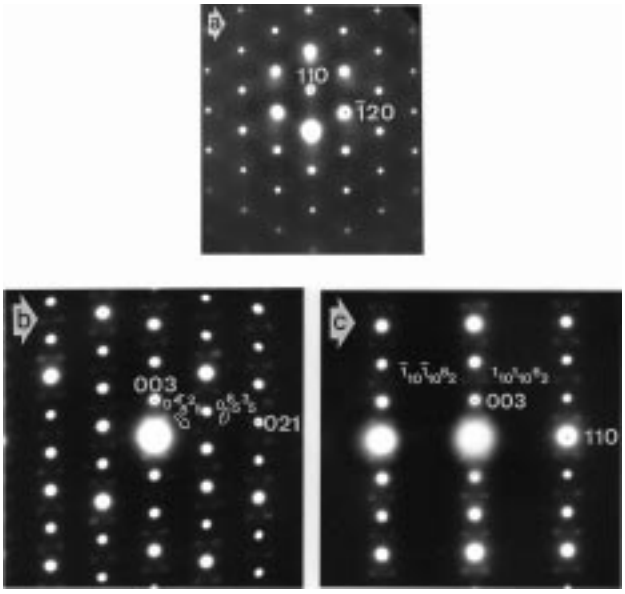

Figure 1. Selected area electron diffraction (SAED) patterns along (a) [001], (b) [100], and (c) [1$\bar{1}$0] zone axes.

Experimental Section

The sample of nominal composition $Ba_3MoNbO_{8.5}$ was prepared from stoichiometric amounts of $BaCO_3$ (Aldrich, 99.98%), Nb_2O_5 (Aldrich, 99.5%), and MoO_3 (Aldrich, 99.5%). After grinding, the powder was pressed into a pellet. This pellet was heated at 1100 °C for 7 days in air, and the homogeneous pale brown product obtained was slowly cooled to room temperature in the platinum crucible used for synthesis.

Thermogravimetric analysis developed on the basis of a CAHN D-200 electrobalance was used to determine the oxygen content, the sample being reduced under H_2 at 900 °C. The total amount of barium, niobium, and molybdenum was determined by inductive coupling plasma (ICP) as well as by EDS X-ray microanalysis carried out on a STEM JEOL 2000FX electron microscope.

Powder X-ray diffraction was performed on a Philips X'Pert diffractometer equipped with a bent copper monochromator and using Cu Kα radiation.

The samples for electron microscopy were ultrasonically dispersed in *n*-butanol and transferred to carbon-coated copper grids. Selected area electron diffraction (SAED) was carried out on a JEOL 2000FX electron microscope. High-resolution electron microscopy (HREM) was performed on a JEOL 4000EX electron microscope.

Results and Discussion

The X-ray diffraction pattern revealed a single-phase sample for the nominal composition $Ba_3MoNbO_{8.5}$. The whole pattern could be identified with the 9R polytype, and it was indexed on a hexagonal lattice with cell parameters $a = 0.593$ nm and $c = 2.101$ nm. However, the electron diffraction study showed the existence of a superstructure.

Figure 1a corresponds to the electron diffraction pattern along the [001] zone axis. It exhibits the geometry distribution consistent with the structure of the BaO_3 layers, and only the reflections with $-h+k+l = 3n$ can be observed. The presence of streaking along the [110]* and equivalent reciprocal directions is also evident and it will be further discussed.

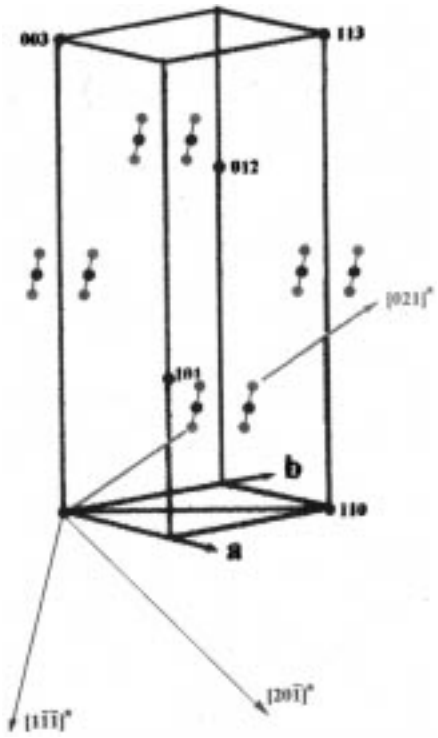

Figure 2. Reciprocal lattice for $Ba_3MoNbO_{8.5}$. Shown are the diffuse diffraction effects in the form of rods as well as the three pairs of superstructure spots which define them, as they are observed in the electron diffraction patterns.

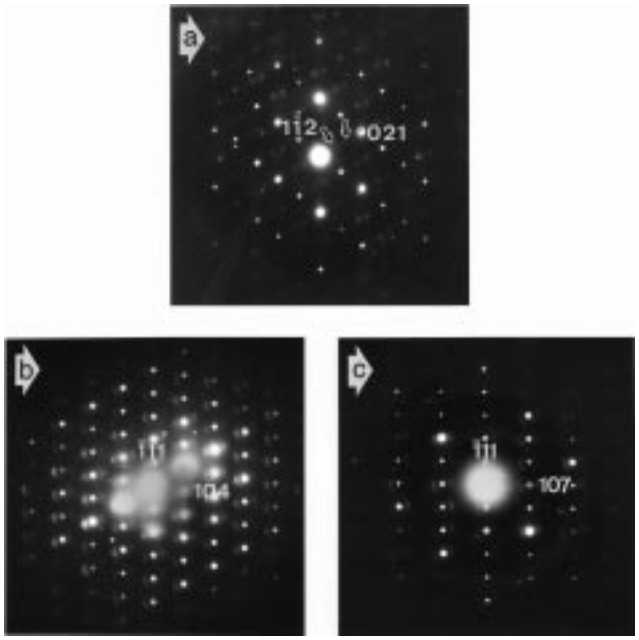

Figure 3. SAED patterns along (a) [51$\bar{2}$], (b) [45$\bar{1}$], and (c) [781] zone axes.

Observing the [100] zone axis (Figure 1b), the spots belong to two classes of intensities. Again, the set of intense diffraction maxima corresponds to the stacking of the BaO_3 layers, the separation of these basic spots being divided into three equal intervals. Superimposed on the basic rhombohedral structure, weak extra reflections are also observed in this pattern at ($^{04}/_{5}{}^{2}/_{5}$) and ($^{06}/_{5}{}^{3}/_{5}$), which is equivalent to considering these spots

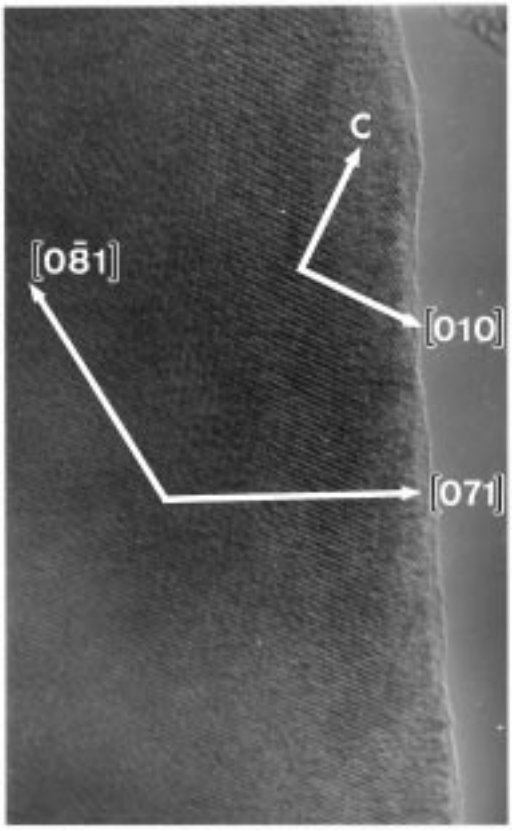

Figure 4. High-resolution electron micrograph of $Ba_3MoNbO_{8.5}$ taken along the [100] zone axis. To enhance the modulation contrast, the negative film was slightly tilted when the photograph was made.

as satellites of the former class with a vector $\mathbf{q} = {}^2/_5[021]^*$. The same extra features are observed in the [010] zone axis, the weak reflections appearing in this case at $({}^4/_5\ 0\ -{}^2/_5)$ and $({}^6/_5\ 0\ -{}^3/_5)$ and $\mathbf{q} = {}^2/_5[20\bar{1}]^*$. Tilting around c^*, the [1$\bar{1}$0] zone axis (Figure 1c) shows pairs of satellite reflections parallel to [110]*. The measurement of the separation between splitted spots corresponds to ${}^1/_5[110]^*$, and the maxima are located at $({}^1/_{10}\ {}^1/_{10}\ {}^l/_2)$ and $({}^{\bar{1}}/_{10}\ {}^{\bar{1}}/_{10}\ {}^l/_2)$, $l = 3n$ and n odd.

Thus, the three most relevant zone axes of the hexagonal structure reveal the presence of three pairs of superstructure spots in such a way that they form two different sets constituted by three aligned diffraction maxima parallel to the [1$\bar{1}\bar{1}$]* direction (see Figure 2).

When the satellite reflections are viewed in reciprocal sections that do not contain the c^* axis, it is seen that they are not discrete spots but rods of diffuse intensity following the [1$\bar{1}\bar{1}$]* direction, and the corresponding SAED patterns deserve additional comment. For example, the [51$\bar{2}$] diffraction pattern (Figure 3a) shows the extra reflections along [021]* to be slightly elongated. This effect is more evident on the reciprocal planes containing the [1$\bar{1}\bar{1}$]* direction. In this sense, a set of rods is observed in both [45$\bar{1}$] and [78$\bar{1}$] zone axes (Figure 3, panels b and c, respectively), the elongation being directed along [1$\bar{1}\bar{1}$]*. At this point it is worth mentioning that these satellites are observed in most of the crystals whether the crystal orientation may be[14] but with variable intensities.

An exhaustive study as well as the reconstruction of the reciprocal space gives rise to superstructure reflections in the form of pairs of rods elongated parallel to the [1$\bar{1}\bar{1}$]* direction and defined by the diffraction spots at $({}^{-1}/_5\ 0\ (l{+}{}^1/_5))$ and $(0\ {}^{-1}/_5\ (l{-}1/5))$ for one rod and at $({}^1/_5\ 0\ (l{-}{}^1/_5))$ and $(0\ {}^{-1}/_5\ (l{+}{}^1/_5))$ for the other.

Such definition originates two segments of magnitude ~2.5 nm (see Figure 2).

As we have previously mentioned, the thermogravimetric analysis confirms the anionic composition to be $O_{8.5}$. The oxygen defect with respect to the 9R polytype

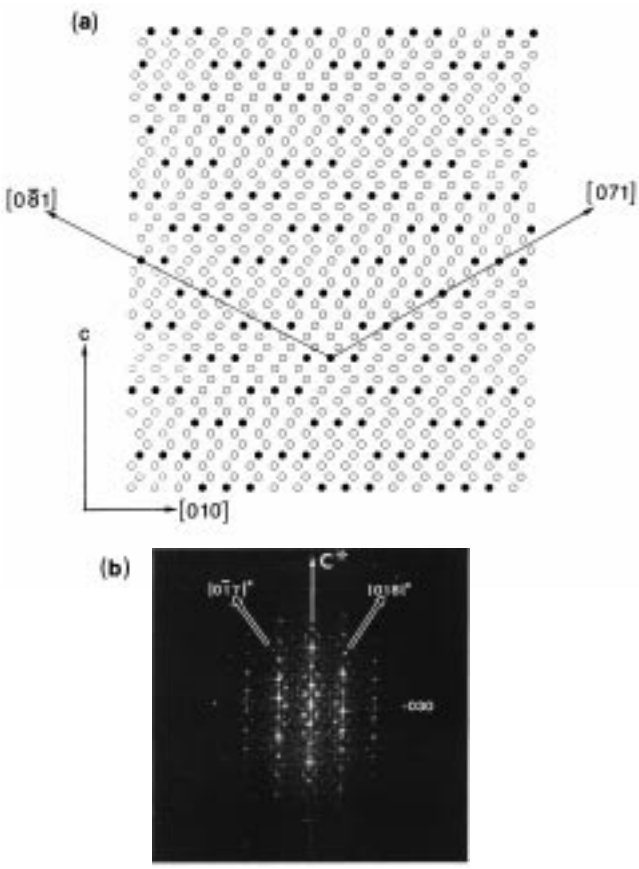

Figure 5. (a) Schematic representation of the contrast distribution observed in the experimental image shown in Figure 4. (b) Corresponding optical diffraction pattern.

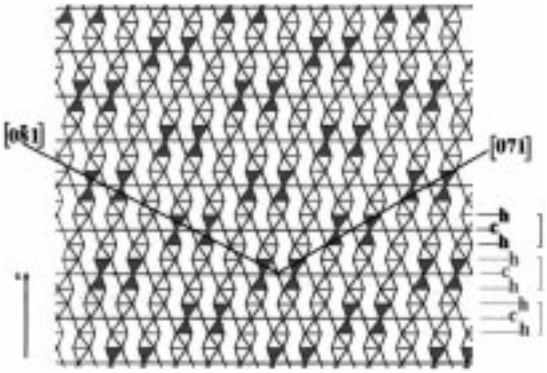

Figure 6. Ideal structural model proposed in the [100] projection. Green polyhedra represent the ordered, distributed tetrahedra at both sides of every c layer. Note that the schematic leads the tetrahedra to share the apical oxygen when in fact it is not shared, as is shown in Figure 7.

(14) Exceptions are the (001)* reciprocal plane and all the planes defined by the reciprocal directions $[h_1k_1l_1]$ and $[h_2k_2l_2]$ such that $(l_1 - l_2) < 3n$.

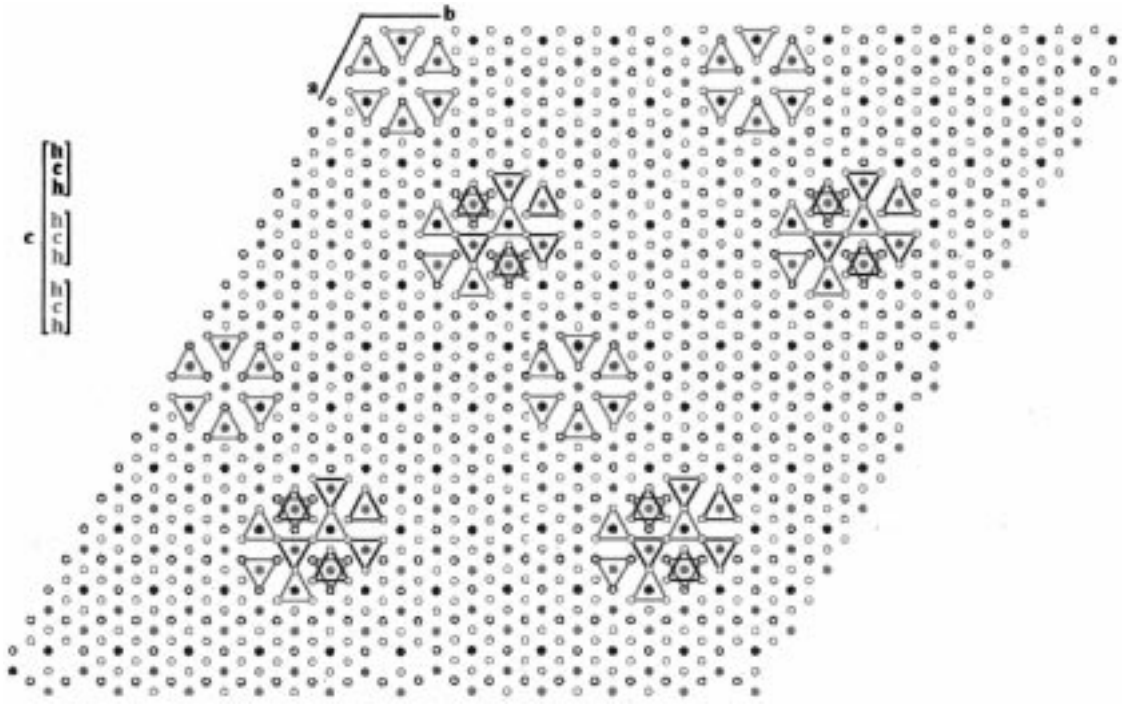

Figure 7. Proposed idealized model, drawn in the [001] projection.

implies that 50% of the metallic atoms in B positions change their coordination number from six (octahedral site) to four (tetrahedral site), and we assume this change does not occur randomly. The arrangement of both types of polyhedra, that is, the replacement of a certain portion of the BaO_3 layers by BaO_{3-x} in a ordered way, is then associated with the satellite reflections observed in the reciprocal lattice.

Therefore, although oxygen positions are usually not revealed in high-resolution images, the most informative images are those taken along zones parallel to the close packing direction of the layers. Figure 4 shows the HREM image of $Ba_3MoNbO_{8.5}$ along the [100] zone axis. It directly reveals the stacking of the close-packed Ba−O layers ($(hhc)_3$ sequence). Besides the 9R average structure, fringes along $[0\bar{8}1]$ are clearly seen under careful observation in the whole crystal. The appearance of this kind of fringe is characteristic of a modulated structure. The distance between fringe corresponds to $5d_{018}$ (∼1.2 nm); this distance coincides with the periodicity of the satellite reflections observed in the corresponding diffraction pattern (see Figure 1b).

The examination of the image contrast shows the BaO_{3-x} cubic layers to be formed by alternating of bright and dark dots in a 3:2 ratio. The regular shifting in the distribution of contrast from one cubic layer to the next giving rise to this characteristic aspect with collapsed segments, that is, the shearing of the structure along **c**, is responsible for the appearance of the fringes mentioned above. The same contrast variation generates also a second set of fringes that corresponds to a modulation along the [071] direction (Figure 4). We will see that these observations may have relevance for the occurrence of the weak extra reflections in the electron diffraction pattern of Figure 1b.

We have made use of optical simulation to derive the diffraction effects in the reciprocal plane [001]. Figure 5a represents, in a schematic way, the contrast distribution in the desired projection. Black and white dots in a 3:2 ratio alternate in one of every three Ba−O layers, i.e., in the cubic layers, in such a way that one layer is shifted along the $[0\bar{8}1]$ or the [071] direction with respect to the next. This optical mask enables a satisfactory comparison between the experimental and the corresponding optical diffraction pattern (Figure 5b).

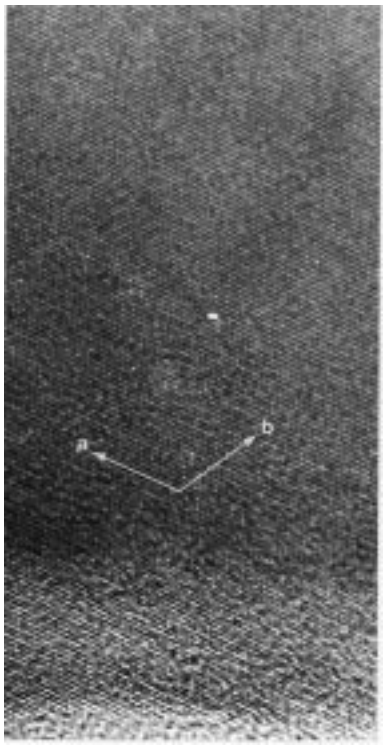

Figure 8. HREM image of $Ba_3MoNbO_{8.5}$ taken along the [001] zone axis. Note the disordered contrast observed along both the **a** and **b** directions.

We interpret the superstructure observed as due esentially to ordering of tetrahedra and octahedra in the

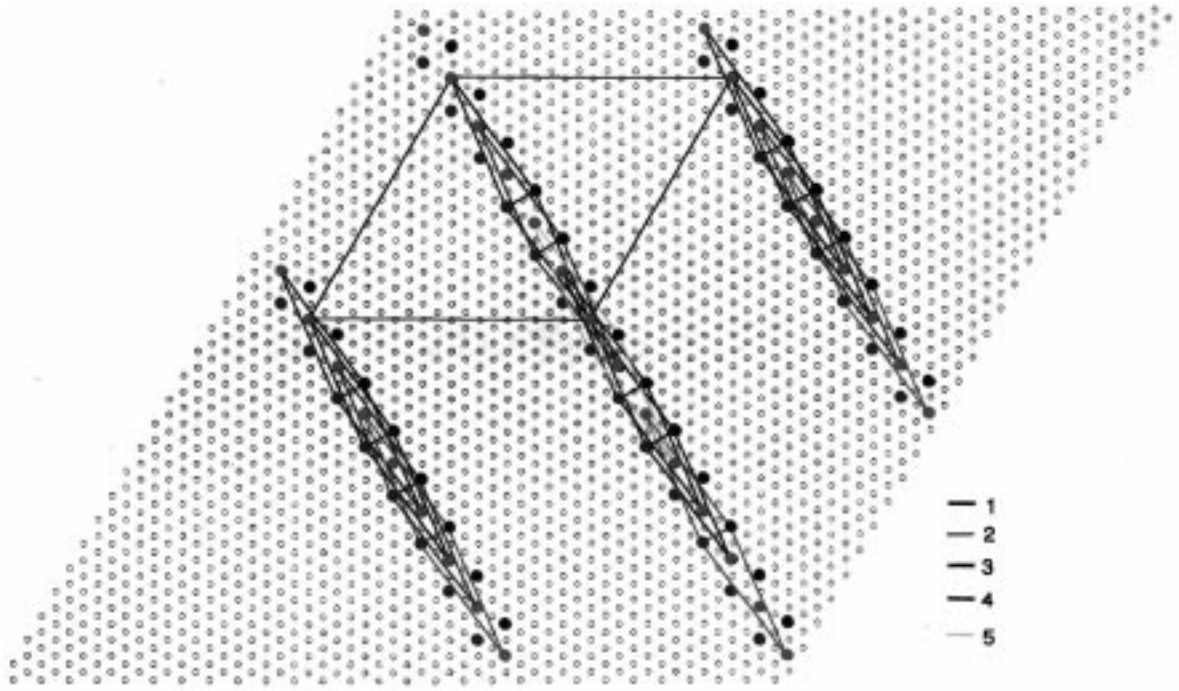

Figure 9. Simplified illustration of the [hch] blocks overlapping along the *c* axis. Large colored circles represent the hexagonal layouts of tetrahedra, and their colors have the same meaning as in Figure 7. Boundaries surrounding the quadrilateral domains have been drawn in different colors. Correlative numbers correspond to differences of $^1/_3c$ when growing up in *z*.

cubic layers. Figure 6 shows an ideal representation of the model proposed in the [100] projection. The transformation from the 9R polytype involves the replacement of the BaO_3 cubic layer of the sequence $(hhc)_3$ by a layer of composition $BaO_{2.6}$. This fact, together with the alternation of the contrast observed, is in agreement with the ordered distribution of octahedra and tetrahedra in a 3:2 ratio. The ordering actually observed is not so well developed and can be approximated by a sinusoidal modulation model affecting the oxygen occupation factor in such layers and probably associated with a significant displacement of the surrounding barium atoms.

The projection along the *c* axis for this idealized model is illustrated in Figure 7. The circles represent the barium and oxygen atoms in a three-layer sequence (hch) like the blocks marked on Figure 6. Inside every block, tetrahedra constitute groups of 6 units in a hexagonal arrangement. The tetrahedral apical oxygen atoms located in the c layer (colored red) are shared with the adjacent octahedra, probably leading to distorted polyhedra. The three oxygen atoms forming the basal plane of the tetrahedra belong to the upper h layer for three of them (colored black) and to the lower h layer for the other three (colored green). Polyhedra so described are marked in red in Figure 7, and such a distribution is repeated every 5 units along both the *a* and *b* axes.

The two adjacent (hch) blocks that would complete the 9-layer sequence of the 9R polytype are equivalent, and the corresponding tetrahedra have been represented in Figure 7 in green and black for the lower and upper blocks, respectively. In addition, one block is shifted with respect to the next, two units and a half along the [110] direction. The first and the third block are displaced along the $[1\bar{1}\bar{1}]$ direction when moving $^2/_3c$.

The alternation of contrast referenced above is not evident in the (001) plane (see Figure 8) as a consequence of the overlapping of enough shifted blocks along *c* to constitute the habitual crystal thickness (7−10 nm). It is reflected, however, in the diffuse streaking observed in the corresponding electron diffraction pattern (Figure 1a).

The *ab* projection of the proposed model has also been used to illustrate the appearance of pairs of diffraction rods parallel to the $[1\bar{1}\bar{1}]^*$ direction. Figure 9 is an extensive and simplified representation of the block overlapping shown previously wherein large circles substitute the hexagonal layouts of tetrahedra (the colors code is the same as in Figure 7). The arrangement constituted by three consecutive blocks can be described as forming quadrilateral domains, and the boundaries surrounding them have been emphasized by colored heavy lines (the five different colors numbered in the figure indicate the *z* coordinate of the *c* layer of each block) as well as the corresponding diagonals that give rise to the small segments shown in the figure. It can be observed that the ordered domains occurs in one of every five $(1\bar{1}\bar{1})$ planes. Such domains share corners along the [110] direction, but they are not connected inside the $(1\bar{1}\bar{1})$ planes. In fact, when moving parallel to the $[1\bar{1}\bar{1}]$ direction and growing up in *z* (that is, changing from one color to the next), one can appreciate isolated rows of domains perfectly ordered in this idealized model. Actually, the order is not so well established and the corresponding diffraction effects are diffuse, and their rodlike nature indicates a lack of long-range order correlations between $\{1\bar{1}\bar{1}\}$ planes with anionic deficiency. The average correlation length is ∼2−3 nm.

According to the preceding discussion, the (hch) sequence of every block of the three constituting the 9R basic cell corresponds to the $BaO_3-BaO_{2.6}-BaO_3$ layer stacking arrangement, since two of every five octahedra have been replaced by tetrahedra at both sides of each cubic layer. The resulting anionic composition is $O_{8.6}$

instead of $O_{8.5}$ as determined by thermogravimetric analysis. Taking into account both the disagreement with the experimental value and the fact that the extra features of the reciprocal lattice are present in every crystal, although with variable intensities, one can assume that in certain areas of the crystals the anionic composition is lower than $O_{8.5}$, without introducing modifications, with respect to 9R, detectable by electron diffraction.

In this sense, and to preserve the basic structural characteristics of the 9R polytype, regions of palmierite structure, that is, O_8 anionic composition, can coexist. Several attempts to obtain intermediate anionic compositions between $O_{8.5}$ and O_8 by reducing the raw material in a controlled atmosphere were unsucessful. The process gave rise always to the partial decomposition of the starting material, with the reduction process leading to the formation of niobium-rich palmierite and the evolution of molybdenum from the precursor.

These experiments support the assumption that certain areas of palmierite are present and that they are probably associated with higher niobium content.

A simple estimation from the difference between the experimental and theoretical anionic vacancies permits us to conclude that the average oxygen content corresponds to 85% of the material constituted by the new ordered phase and the remaining 15% to palmierite.

The important chemical effect apparent in this work is that the mode of accommodating a substantial oxygen deficiency is by insertion of a different block arrangement rather than by random point defects. From a structural point of view, one can say that the relative flexibility of the $(hhc)_3$ stacking sequence to incorporate anionic nonstoichiometry leads to the formation of a modulated structure through an ordered shearing mechanism along c, by introducing mixed $BaO_{2.6}$ cubic layers in the 9R polytype.

Acknowledgment. We acknowledge the financial support of CICYT (Spain) through Research Project MAT95-0642. We are also grateful to the Centro de Microscopía Electrónica (UCM) for facilities, and specially to E. Baldonedo for valuable technical assistance.

CM9708022